A Physical Model for GPS Multipath Caused by Land Reflections: Toward Bare Soil Moisture Retrievals

Valery U. Zavorotny, *Senior Member, IEEE*, Kristine M. Larson, John J. Braun, Eric E. Small, Ethan D. Gutmann, and Andria L. Bilich

***Abstract*—Reflected Global Positioning System (GPS) signals can be used to infer information about soil moisture in the vicinity of the GPS antenna. Interference of direct and reflected signals causes the composite signal, observed using signal-to-noise ratio (SNR) data, to undulate with time while the GPS satellite ascends or descends at relatively low elevation angles. The soil moisture change affects both the phase of the SNR modulation pattern and its magnitude. In order to more thoroughly understand the mechanism of how the soil moisture change leads to a change in the SNR modulation, we built an electrodynamic model of GPS direct and reflected signal interference, i.e., multipath, that has a bare-soil model as the input and the total GPS received power as the output. This model treats soil as a continuously stratified medium with a specific composition of material ingredients having complex dielectric permittivity according to well-known mixing models. The critical part of this electrodynamic model is a numerical algorithm that allows us to calculate polarization-dependent reflection coefficients of such media with various profiles of dielectric permittivity dictated by the soil type and moisture. In this paper, we demonstrate how this model can reproduce and explain the main features of experimental multipath modulation patterns such as changes in phase and amplitude. We also discuss the interplay between true penetration depth and effective reflector depth. Based on these modeling comparisions, we formulate recommendations to improve the performance of bare soil moisture retrievals from the data obtained using GPS multipath modulation.**

***Index Terms*—Coherent scattering, global positioning system (GPS), reflectivity, soil moisture.**

I. Introduction

In [1] and [2], it was demonstrated that GPS receivers installed primarily for geophysical and geodetic applications can also be used to estimate variations in near surface soil moisture. This is possible because of three major factors. First, the antenna gain pattern of such GPS receivers is not confined to positive elevation angles. Despite the attempts of antenna designers to maximize direct signal reception while also minimizing susceptibility to surface multipath, there is still a sizable gain at negative angles which makes it possible for a GPS receiver to intercept radio waves from ground reflections. Second, the antennas of the GPS receivers under consideration are installed at relatively low heights, $h \sim 2$ m above the ground. This leads to a short time delay between direct and reflected signals, well within a single pseudo-random modulation code length, therefore allowing these two signals to freely interfere at the antenna location. Third, the L-band (1.57542 and 1.22760 GHz) GPS signals are also sensitive to variations of the dielectric constant of land (e.g., [3]), which in turn is determined by the near-surface soil moisture, together with other parameters of the soil. That is why L-band radiometers are considered more suitable for soil moisture measurements than radiometers employing shorter wavelengths (e.g., [4]).

When the above-mentioned GPS receivers receive both direct and reflected signals, the output signal power, or signal-to-noise ratio (SNR), as a function of time (or the GPS satellite's elevation angle) manifests a quasi-periodic oscillating pattern resembling a phenomenon of light intensity fringes in optical interferometers [Fig. 1(a)]. These oscillations are created by the phase offset between direct and reflected signals, and is a function of the distance to the reflector h and the GPS wavelength λ. For a flat, horizontal surface at the antenna site, the phase offset Φ is equal to $k\Delta l = 2kh\sin\theta$, where $k = 2\pi/\lambda$, Δl is the difference in path lengths between the direct and reflected signal, and θ is the satellite elevation angle.

After the dominant direct signal power trend is subtracted from the total signal, there is an optimal range of elevation angles where the effect of multipath interference is most pronounced [Fig. 1(b)]. Those elevation angles θ commonly reside between several degrees and 30°–40°. At very low grazing angles, the path difference tends to zero, therefore halting the modulation.

The most visible effect of soil moisture change on experimental SNR modulation patterns is stretching (frequency change) or shifting (phase change) the pattern with respect to time or elevation angle [Fig. 1(b)]. Intuitively, this effect can be thought of as changing the antenna height above the reflecting surface; a height change would create an additional phase shift between carriers of the direct and reflected waves, which would then lead to a shift in the phase of the modulation pattern. At the same time, it is known that the penetration depth of L-band radio waves into the soil depends on soil absorption which

Manuscript received August 28, 2009; revised September 16, 2009. This work was supported in part by the University of Colorado Seed Grant Competition, NSF ATM 0740515 (CU) and NSF ATM 0740498 (UCAR). NCAR is supported by the National Science Foundation.

V. U. Zavorotny is with the Earth Systems Research Laboratory, National Oceanic and Atmospheric Administration, Boulder, CO 80305 USA (e-mail: valery.zavorotny@noaa.gov).

K. M. Larson is with the Department of Aerospace Engineering Sciences, University of Colorado, Boulder, CO 80309 USA (e-mail: kristinem.larson@gmail.com).

J. J. Braun is with COSMIC, University Corporation for Atmospheric Research, Boulder, CO 80301 USA (e-mail: braunj@ucar.edu).

E. E. Small is with the Department of Geological Sciences, University of Colorado, Boulder, CO 80309 USA (e-mail: eric.small@colorado.edu).

E. D. Gutmann is with Research Applications Laboratory, National Corporation for Atmospheric Research, Boulder, CO 80307 USA (e-mail: gutmann@ucar.edu).

A. L. Bilich is with the National Geodetic Survey at the National Oceanic and Atmospheric Administration, Boulder, CO 80305 USA (e-mail: andria.bilich@noaa.gov).

Digital Object Identifier 10.1109/JSTARS.2009.2033608

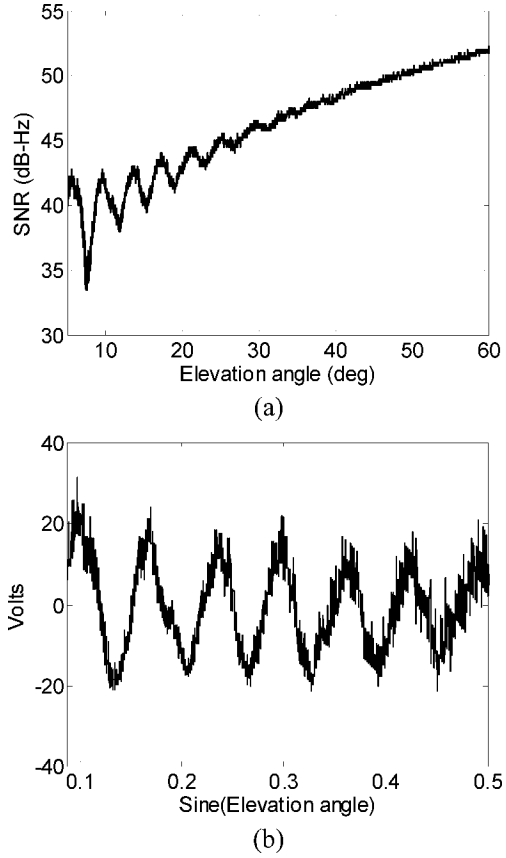

Fig. 1. (a) Raw SNR data from a NetRS Trimble receiver for PRN 13; (b) corresponding detrended SNR data at low elevation angles.

increases when soil becomes moister [3]. At first glance, the notion of an effective reflector appropriately positioned beneath the actual surface would be enough to describe the modulation pattern and its temporal evolution. However, a secondary feature is also present in experimental SNR data, a change in amplitude. The peak-to-peak amplitude of the modulation is another characteristic of this phenomenon which indicates that not only the penetration depth but also the reflection strength is changing with soil moisture. In order to quantify the reflection strength we need to build an electrodynamic model of GPS multipath that would have a soil model as an input and the GPS total received power as a function of the satellite elevation angle as an output.

To build the model, we first take into consideration that the GPS signal acquires some degree of depolarization upon reflection for a dielectric medium such as soil. By design, the transmitted GPS signal has primarily right-hand circular polarization (RHCP) with an ellipticity no worse than 1.2 dB for L1 signal and 3.2 dB for L2 signal within an angle of $\pm 14.3^{\circ}$ from boresight (see, e.g., [5, p. 84]). The reflected wave consists of both RHCP and left-hand circular polarization (LHCP) components due to partial depolarization upon reflection from the surface [6]. The amplitude and phase of those two types of waves depends on both incidence angle and the dielectric properties of the soil. Second, the soil cannot be considered as a uniform medium with a constant dielectric permittivity. Even the simplest bare soil model requires the assumption of soil dielectric permittivity dependence with depth, and a relationship between the soil dielectric permittivity and soil moisture, as well as soil material composition [7]–[9]. Here, we employ a well-known approach [10]–[15] that allows calculation of electromagnetic field reflection coefficients from a continuously stratified medium with known profiles of dielectric permittivity. The soil dielectric profiles for the specific sites used in observations [1], [2] are obtained employing semiempirical dielectric mixing models [7]–[9].

In this paper, we present a physical model based on a bare soil/flat surface assumption that reproduces the main features of the multipath modulation patterns obtained with commonly used geodetic antennas under soil conditions described in [1], [2]. At this point, we do not account for the effects of vegetation and surface topography or roughness on the GPS multipath modulation since the problem of modeling GPS signal reflection from a bare soil/flat surface is sufficiently complex and important to be considered separately. Vegetation and roughness conditions at the experimental site [1], [2] were favorable for comparisons with the bare soil/flat surface model. Based on these modeling results, we formulate recommendations to improve the performance of soil moisture retrievals from the data obtained using GPS multipath modulation under bare soil/flat surface conditions.

II. Derivation of the Expression for a GPS Signal Affected by the Surface Multipath

Here, we obtain basic expressions for the correlation power of a GPS signal under conditions of single-reflection multipath propagation. This situation takes place when the antenna height above the ground is small enough so that both radio waves, the direct one and the one reflected from the ground, sum at the antenna point coherently, well within the GPS code time interval, called a "chip." For the coarse/acquisition (C/A) code considered here, this is equal to 10^{-6} s. The geometry of the problem is shown in Fig. 2. Because of the great distance to the GPS satellite ($> 20{,}000$ km), the incoming radio wave can be treated as a plane wave. We limit ourselves to the case of a horizontal planar ground surface with a layered soil beneath it; i.e., its dielectric permittivity depends only on the vertical coordinate, z. In this case, the plane wave reflected from the plane ground in a specular direction is a plane one as well. To this end, surface roughness ζ with r.m.s. height σ_ζ can be incorporated by introducing a coherence loss factor $\exp(-k^2\sigma_\zeta^2 \sin^2\theta/2)$ into an expression for the reflected signal. For small values of the Rayleigh parameter, $k\sigma_\zeta \sin\theta$, the reflected wave preserves its coherence, allowing complete interference with the direct wave. For the conditions reported in [2], this parameter seems to be small since the interference effect is very pronounced.

As mentioned above, the incoming, direct GPS signal is primarily of right-hand circular polarization (RHCP), whereas the reflected signal due to depolarization has both RHCP and left-hand circular polarization (LHCP). Commonly used GPS antennas are designed to suppress signals arriving at low positive and negative elevation angles to mitigate ground multipath. As a result, the antenna gain for RHCP and LHCP at those angles are comparable or even tend to be in reverse. Since our problem is concerned with a multipath propagation regime of the signal,

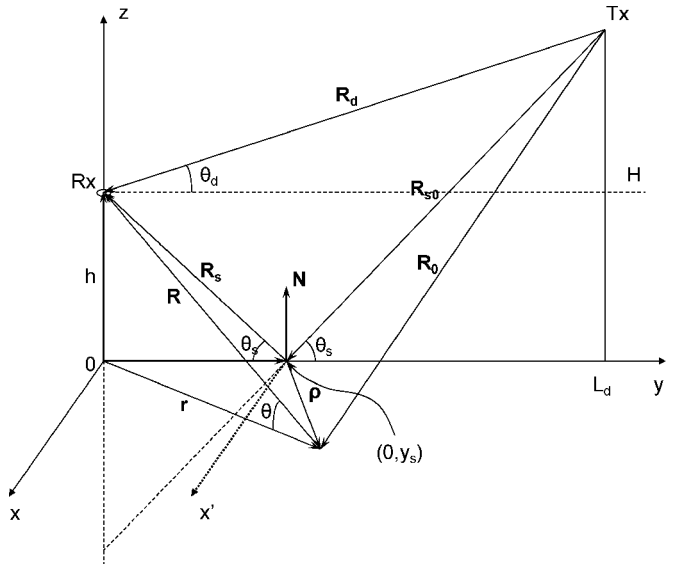

Fig. 2. Geometry of the problem.

both polarization components arriving at the antenna should be considered.

We begin assembling the model of signal power by assuming that the power transmitted by the GPS satellite antenna equals to unity. Under this condition, the complex amplitude u of the GPS spread-spectrum signal obtained from the output of the GPS receiving antenna can be expressed as $u(t) = u_0(t)\exp(ikR_d - 2\pi i f_c t)a(t - R_d/c)/R_d$, where $a(t)$ is a pseudo-random-noise (PRN) biphase-coding function, R_d is a distance between the GPS transmit and receive antennae, c is the speed of light, $k = 2\pi f_c/c$, f_c is a carrier frequency of the GPS signal. Factor u_0 is a complex function (a phasor) that accounts for slow (compared with the carrier oscillations) signal changes, as a function of the GPS satellite elevation angle. This factor captures amplitude changes due to both the passage of the direct and reflected signals through the receive antenna pattern and attenuation due to ground multipath.

In the GPS receiver, the received signal u obtained from the antenna output at a time $t_0 + \tau$ is cross correlated with a local replica $a\,(t)$ of the PRN code taken at a different time t_0 multiplied by the oscillation factor $\exp(2\pi i f_c t')$ (cf., [12])

$$Y\,(t_0, \tau) = \int_0^{T_i} u\,(t_0 + t' + \tau)\,a\,(t_0 + t')\exp(2\pi i f_c t')dt'. \tag{1}$$

The GPS receiver performs a search for the peak of the cross-correlation $Y_{\rm peak}\,(t_0) = Y\,(t_0, \tau_{\rm peak})$ by changing the time lag τ. It can be shown that the demodulation and despreading of the original signal performed in (1) produces $Y_{\rm peak}\,(t_0)$, which is a slow function of time t_0 (or, rather, an elevation angle), and is proportional to phasor u_0. In what follows, we will omit t_0 for simplicity.

For a receive antenna located near a flat surface, the composite signal tracked by the receiver is the sum of two signals, direct and reflected. In this case, phasor u_0 is also a sum of two components

$$u_0 = u_{0,\rm dir} + u_{0,\rm ref}. \tag{2}$$

Then, for the instantaneous peak correlation power $P_{corr}(t_0) = |Y_{\rm peak}(t_0)|^2$ we have

$$P = |u_0|^2 = |u_{0,\rm dir} + u_{0,\rm ref}|^2. \tag{3}$$

A factor $\exp\left[i\Phi(\theta)\right]$ associated with the phase shift $\Phi = k\Delta l = 2kh\sin\theta$ due to difference Δl between geometric paths for the direct and reflected signals can be explicitly extracted from $u_{0,\rm ref}$

$$u_{0,\rm ref} = u_{1,\rm ref}\exp\left[i\Phi(\theta)\right]. \tag{4}$$

Equation (4) does not yet explicitly show terms for antenna pattern and the surface reflectivity, which we require for our model. Let us introduce a complex quantity

$$A = 2u^*_{0,\rm dir}u_{1,\rm ref} = 2\left|u^*_{0,\rm dir}u_{1,\rm ref}\right|\exp\left[i\Psi\,(\theta)\right] \tag{5}$$

from which argument $\Psi\,(\theta)$ can be retrieved by the following procedure:

$$\Psi\,(\theta) = \tan^{-1}\left(\frac{\mathrm{Im}\,A}{\mathrm{Re}\,A}\right). \tag{6}$$

Now, substituting (4) into (3) and making use of (6) in (3), we obtain for the power P the following expression:

$$P = |u_{0,\rm dir} + u_{0,\rm ref}|^2 = |u_{0,\rm dir}|^2 + |u_{1,\rm ref}|^2 + 2\left|u^*_{0,\rm dir}u_{1,\rm ref}\right|\cos\left[\Phi\,(\theta) + \Psi\,(\theta)\right]. \tag{7}$$

Equation (7) represents a modulation pattern having a characteristic oscillating structure caused mainly by the geometric phase delay Φ describing interference between direct and reflected waves. An additional term $\Psi\,(\theta)$ describes phase effects of antenna pattern and the surface reflectivity. In order to determine Ψ we need to calculate complex phasors $u_{0,\rm dir}$ and $u_{1,\rm ref}$ related to direct and reflected signals, respectively.

An output of the antenna $u_{0,\,\rm dir}$ generated by the direct signal from a satellite at elevation angle θ is a simple function of the incident phasor u_0 and the antenna radiation pattern F

$$u_{0,\,\rm dir}(t) = u_0 F(\theta). \tag{8}$$

We find that for the accuracy level of our estimations, the incoming direct GPS signal can be regarded as a perfectly RHCP radio wave [5]. Here, $F = F_R$ is the GPS antenna radiation pattern at RHCP.

In general, F can be treated as a complex function of elevation and azimuth angles. The argument or phase of this complex function describes the effective phase center of the antenna, or the departure of the antenna phase front from a sphere. In the case of the receiving antenna, the absolute value (modulus), or

amplitude, of F describes the strength of the received electromagnetic field at the specific angle. In terms of power units, $|F|^2$ is equivalent to the antenna gain G. The design of commercially built GPS antennas is such that the gain at RHCP for positive elevation angles (the upper hemisphere) is significantly higher than for negative elevation angles (the lower hemisphere) in order to minimize the adverse effect of ground multipath. Similarly, the antenna gain at LHCP, G_L, it is designed to be lower than the gain at RHCP over all elevation angles. Although these antennas are optimal for receiving primarily direct GPS signals, they are not optimal at all for soil moisture sensing purposes. However, we consider here this type of antenna because it is used widely by surveying, geophysical, and meteorological networks [1], [2]. Despite these difficulties, it is still possible to measure signal modulations due to ground multipath and use it for soil moisture measurements as was shown in [1].

The complex amplitude of the reflected field $u_{\mathrm{ref},n}$ can be expressed through the diffractional integral over the land surface area limited to a so-called annulus zone [6] dictated by the length of the GPS signal code, centered on a specular point. The analysis of that integral, taken in a Kirchhoff approximation (see, e.g., [10]), shows that for the case of L-band radio waves, for the ideally planar surface and the transmitter-receiver geometry considered here, the incoming wave can be expanded into plane waves, and this diffraction integral can be further calculated in the form of the main, geometric optics terms. A correction to the geometric optics field expression depends on the first and second derivatives of the plane-wave reflection coefficient over the incidence angle taken at the specular point. In the case of an ideally conductive plane, the reflection coefficient does not depend on the angle of incidence; therefore, correction terms are exactly equal to zero. For the case of the finite-conductive, lossy medium the reflection coefficient does depend on the angle of incidence and requires correction terms [10]. However, our calculations show that for conditions adopted here these correction terms are small compared to the main, geometric optics terms. As a result, the geometric optics approximation is applicable here. The main geometric optics contribution comes mostly from a relatively narrow first Fresnel zone around the specular point, which is of the order $\sqrt{\lambda L}$, where L is the distance between the antenna and the specular point [10].

The complex amplitude of the reflected field can be expressed in the geometric optics limit as a product of the complex amplitude of the incident field taken in a specular direction and the local, polarization-dependent reflection coefficient, $V_{m,n}$. The first index, m in $V_{m,n}$, stands for the polarization state of the incident wave, and the second index, n, stands for the polarization state of the reflected wave. In order to proceed from linear polarizations (vertical v and horizontal h) to circular (RHCP R and LHCP L) ones, the following relationships should be used:

$$V_{RR} = V_{LL} = \frac{1}{2}\left(V_v + V_h\right) \tag{9}$$

$$V_{RL} = V_{LR} = \frac{1}{2}\left(V_v - V_h\right). \tag{10}$$

Therefore, for the total reflected signal, one can write the following expressions:

$$\begin{aligned} u_{1,\mathrm{ref}}\left(-\theta\right) &= u_{1,ref,R} + U_{1,ref,L} \\ &= u_0\left[V_{RR}F_R\left(-\theta\right) + V_{RL}F_L\left(-\theta\right)\right]. \end{aligned} \tag{11}$$

Here, we assume that the specular point is seen from the antenna point at angle $-\theta$ (negative of the satellite elevation angle) because the distance R_d from the antenna to the satellite is much greater than the distance R_s to the specular point. A corresponding power, $|u_{1,\mathrm{ref}}|^2$ that enters to the total power in (3) as a second term can be calculated readily from (11). For the modulation term in (3) upon substitution of (11) into (5), we obtain

$$\begin{aligned} A\left(\theta\right) = 2u^*_{0,\mathrm{dir}}u_{1,\mathrm{ref}} &= 2|u_0|^2\exp\left[i\Psi\left(\theta\right)\right] \\ &* \left|F^*_R\left(\theta\right)\left[V_{RR}F_R\left(-\theta\right) + V_{RL}F_L\left(-\theta\right)\right]\right| \end{aligned} \tag{12}$$

where

$$\Psi\left(\theta\right) = \tan^{-1}\left[\frac{\mathrm{Im}\left(F^*_R\left(\theta\right)\left(V_{RR}F_R\left(-\theta\right) + V_{RL}F_L\left(-\theta\right)\right)\right)}{\mathrm{Re}\left(F^*_R\left(\theta\right)\left(V_{RR}F_R\left(-\theta\right) + V_{RL}F_L\left(-\theta\right)\right)\right)}\right]. \tag{13}$$

From (12) and (13), it is seen that both amplitude $|A\left(\theta\right)|$ and phase $\Psi\left(\theta\right)$ of the multipath modulation pattern depend on a combination of soil reflectivity (via V_{RR} and V_{RL}) and antenna gain (at positive and negative elevation angles) at two polarizations. Therefore, the behavior of $|A|$ and $\Psi\left(\theta\right)$ could be rather arbitrary depending on the specific antenna type being used.

It is convenient to represent complex values of reflection coefficients V_{mn} and antenna patterns F_n in the form of their amplitudes and phases ($|V_{mn}|$ and Θ_{mn}, $|F_n|$ and S_n, respectively)

$$V_{mn}\left(\theta\right) = \left|V_{mn}\left(\theta\right)\right|\exp\left[i\Theta_{mn}\left(\theta\right)\right] \tag{14}$$

$$F_n = \left|F_n(\theta)\right|\exp\left[iS_n(\theta)\right]. \tag{15}$$

To make (12) and (13) more compact, we omit θ notation in F_n and S_n, and dependence on negative θ will be indicated by a minus sign at the subscripts, e.g., $F_n(-\theta) = F_{-n}$. Therefore, factors in (12) can be expressed as

$$|A| = \left(A_1^2 + A_2^2\right)^{1/2}, \quad \Psi = \tan^{-1}\left(\frac{A_2}{A_1}\right) - S_R \tag{16}$$

$$A_1 = 2|u_0|^2\left|F_R\right|\left(\left|F_{-R}\right|\left|V_{RR}\right|\cos\beta + \left|F_{-L}\right|\left|V_{RL}\right|\cos\gamma\right) \tag{17}$$

$$A_2 = 2|u_0|^2\left|F_R\right|\left(\left|F_{-R}\right|\left|V_{RR}\right|\sin\beta + \left|F_{-L}\right|\left|V_{RL}\right|\sin\gamma\right) \tag{18}$$

$$\beta = S_{-R} + \Theta_{RR}, \quad \gamma = S_{-L} + \Theta_{LR}. \tag{19}$$

As an example, assume that the reflective medium is a perfect conductor. Then, the reflection coefficient $|V_{RR}|$ becomes zero, and $|V_{RL}|$ becomes 1, whereas phases Θ_{RR}, Θ_{LR} become zero. As a result, we obtain

$$A = 2|u_0|^2\left|F_R\right|\left|F_{-L}\right|\cos\left(S_R - S_{-L}\right). \tag{20}$$

Intuitively, one might expect that since reflection from a perfect conductor is stronger than that from a lossy medium such as soil, the modulation amplitude should also be stronger. However, the comparison between the amplitude factor A from (20) and A_1 and A_2 from (17) and (18) shows that this is not necessarily the

case. For an incoming RHCP wave, it is important to realize how much of this polarization transforms back into the same RHCP wave in order to effectively interfere with the direct wave having the same polarization. In the case of the perfect conductor, a reflected RHCP wave is not generated since $|V_{RR}| = 0$. In contrast, in the case of the lossy medium, $|V_{RR}| \neq 0$, and this significantly enhances A_1 and A_2 from (17) and (18) through the presence of the first terms, especially being multiplied by factors $|F_R(-\theta)|$, which are stronger than factors $|F_L(-\theta)|$ employed in the second terms of A_1 and A_2 . This conclusion is supported by field measurements where the observed multipath amplitude A initially decreases with increased surface soil moisture.

III. Connection Between Measured Soil Moisture Profiles and Reflection Coefficients

The issue of how to produce a dielectric permittivity profile $\varepsilon(z)$ for a specific radio wave band from a soil moisture profile was previously considered for the problem of soil remote sensing using microwave radiometers [3], [4], [7]–[9]. In papers [7]–[9], semiempirical models were proposed for soil dielectric permittivity at various microwave radio frequencies as a function of soil moisture for various types of soil. Here we use empirical relationships developed in [8] that relate real and imaginary parts of ε for L-band to the volumetric water content (VWC) in soil. Note that according to [8], soil dielectric permittivity does not noticeably change over the range of radio frequencies encompassing the GPS L1 and L2 frequencies. Therefore, our conclusions are applicable to both bands. In [8], plots were presented of ε versus VWC for five different types soil: sandy loam, loam, silt loam 1, silt loam 2, and silty clay. The type of soil at Marshall, CO, was classified as a cobbly clay which is heavier than silty clay; we used ε versus VWC for the silty clay soil type from [8] as the closest proxy for our calculations. However, we note that calculations of the modulation pattern using ε versus VWC for other types of soil did not result in a significant difference.

VWC profiles were obtained at Marshall, CO, using Campbell Scientific water content reflectometers (WCR) next to the sites where the GPS reflection experiment [1], [2] was performed. It is known that moisture measurements performed with water content time-domain reflectometers are sensitive to the calibration of these sensors, especially, for soils with significant clay content [16]. We calibrated the WCR probes in the lab with an accuracy of 0.01 VWC using soil collected from the site; this calibration was consistent with VWC measurements from field samples collected at three separate times. Probes were installed at six depths: 2.5, 7.5, 20, 40, 60, 100 cm. The primary criterion for the chosen depths was high resolution near the surface (2.5 and 7.5 cm). Given the averaging thickness of the probes (5 cm) [17], this allows for estimates of soil moisture in the 0–5 and 5–10 cm depth layers. The second criterion was to relate these surface measurements to processes at greater depths (root water uptake, storage, and recharge of groundwater). For this, we chose depths that are consistent with previous studies (see, e.g., [18]) and that would permit comparison to modeled soil moisture profiles (see, e.g., [19]). As a result, these depths were not optimal for modeling soil dielectric permittivity profiles. Data sets of

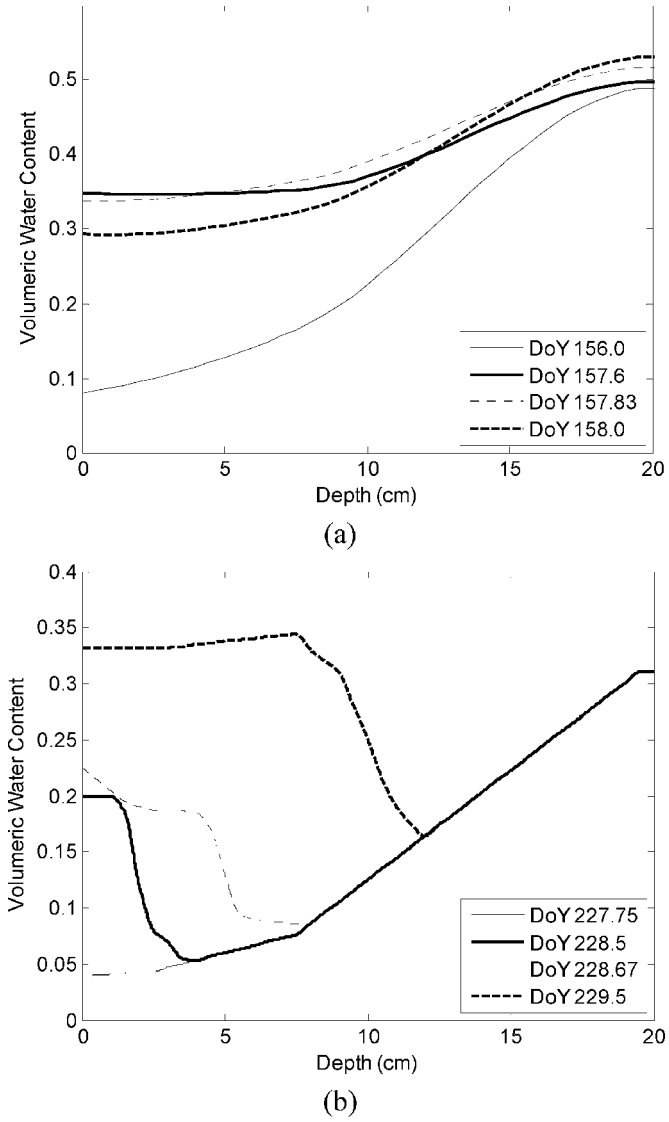

Fig. 3. (a) VWC profiles obtained from measurements during DoY 156.0, DoY 157.6, DoY 157.83, DoY 158.0; (b) VWC profiles obtained from measurements during DoY 227.75, DoY 228.5, DoY 228.67, and DoY 229.5.

VWC were used for the period of summer 2008 that had both dry and wet conditions. Three levels (at 2.5-, 7.5-, and 20-cm depth) were considered as a baseline to create synthetic VWC profiles with the needed depth resolution for depths between 0 and 20 cm for four sequential times over UTC days 156–158, specifically DoY 156 (dry soil, before rain), DoY 157.6, DoY 157.83 (wet soil, during rain), and DoY 158 (wet soil, after rain). Rain began on DoY 156 around 1900 UTC with 5 mm of accumulated precipitation by the end of the day. Rain continued throughout DoY 157, with storm totals equaling 25 mm on that day. Profiles for DoY 156–158 are shown in Fig. 3(a) and represent an interpolation between the three baseline levels and extrapolation toward the surface assuming a smooth wetting front, consistent with the high initial VWC and the top two VWC observations. Since there were no points above the 2.5-cm level, this extrapolation is somewhat arbitrary.

Fig. 3(b) depicts VWC profiles for four times during another precipitation event, specifically DoY 227.75, DoY 228.5, DoY

228.67, and DoY 229.5. The daily precipitation totals for those days are: 14.8 mm on DoY 228, 34.4 mm on DoY 229, and 12.8 mm on DoY 230. On DoY 157, the soil was still wet from spring rain and snows ($\mathrm{VWC} = 0.5$ at 20 cm); the most recent rain event occurred on DoY 148. In contrast, on DoY 228, the soil was dry after over two months with no significant rainfall ($\mathrm{VWC} = 0.3$ at 20 cm); the previous rain event was the event on DoY 157. As a result, on DoY 228 a sharp wetting front formed. So, VWC profiles in Fig. 3(b) were obtained by interpolating from the data at the three depths assuming a sharp wetting front, consistent with low initial VWC and sharp changes between the top two VWC observations.

From these VWC profiles, corresponding profiles of complex dielectric constant (CDC) were obtained based on the model from [8] for various types of soil. In Fig. 4(a) and (b), the real and imaginary components of dielectric constant with depth are plotted for the event around DoY 158 and for the silty clay type of soil. Because CDC is directly proportional to VWC, the complex dielectric profiles behave similarly to the profiles of water content.

Fig. 5(a) and (b) depicts results of computations for reflection coefficients at two polarizations obtained with a layered-medium numerical code. The layered medium is simulated using CDC profiles shown in Fig. 4(a) and (b). Plots are presented for DoY 156 (dry conditions) and DoY 158 (wet conditions). For dry conditions, the amplitude of the RHCP reflection coefficient exceeds the amplitude of the LHCP coefficient over elevation angles below 30°. For wet conditions the amplitude of the LHCP coefficient exceeds the amplitude of the RHCP coefficient between 15° and 30° of the elevation angle. Such a relationship between the amplitudes of reflection coefficients at different polarizations combined with the antenna pattern behavior at the same angles leads to a modulation shift which is demonstrated further. Also note that the phases of reflection coefficients at both polarizations shown in Fig. 5(b) do not change significantly with the angle or with the soil conditions.

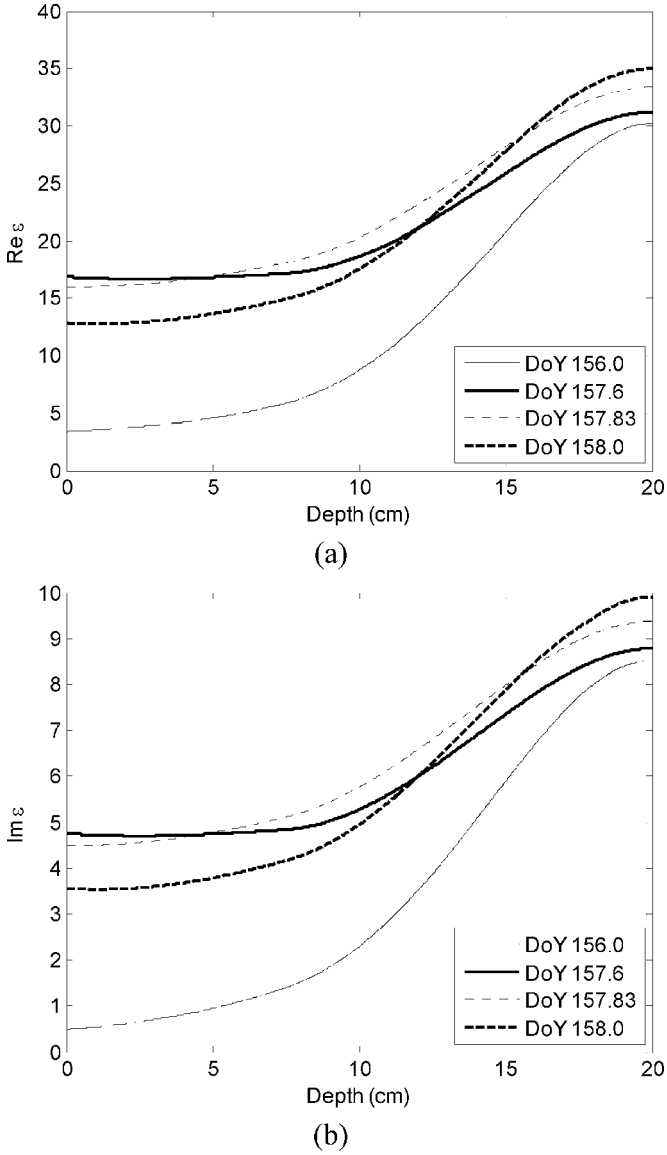

Fig. 4. (a) Real and (b) imaginary part of dielectric permittivity for VWC profiles from Fig. 3.

IV. Results

A. Main Factors Affecting Modulation Pattern

In [1] and [2], it is demonstrated that the modulation of the SNR of the GPS signals received at relatively low elevation angles (see Fig. 1), which are usually considered as nuisance caused by the surface multipath propagation of GPS signals, can be used to measure soil moisture. It is shown that these data are sensitive to soil moisture variations for areas of 1000 m^2 horizontally and 1–6 cm vertically. It is demonstrated that GPS signals penetrate deeper when the soil is dry than when it is wet, which correlates with changes in the dielectric constant of near-surface soil. This change in penetration or "reflector" depth, or the change in dielectric constant, causes the SNR modulation to change its frequency and amplitude.

Comparisons with conventional water content reflectometer sensors show good agreement ($r^2 = 0.9$ to 0.76) with the GPS-derived soil moisture parameter over a period of seven months, with most of the disagreement occurring when soil moisture content is less than 0.1 $\mathrm{cm}^3/\mathrm{cm}^3$.

In order to explain these observations, behavior of the SNR modulation was modeled as a function of various parameters to better understand the dominating factors. We first calculated the SNR modulation dependence on the elevation angle using (3) and (11)–(19); reflection coefficients were produced with a numerical code based on an algorithm similar to one proposed in [15] and dielectric constant profiles described above.

Our calculations also require GPS antenna radiation patterns at two polarizations; we used data sheets for the Trimble L2 choke ring antenna power gain patterns for the range of elevation angles between $+30$ and $-30°$. In this range of angles, the power gain at LHCP is below the corresponding gain at RHCP by 15 to 5 dB. The largest contrast between gains on opposite polarizations is $\sim$ 15 dB at maximum positive angles with a gradual reduction to $\sim$ 5 dB at $-30°$.

Another important characteristic of the antenna pattern F is its phase, or a phase center position, determined by values $S_n(\pm\theta)$ from (15). Unfortunately, information about phase

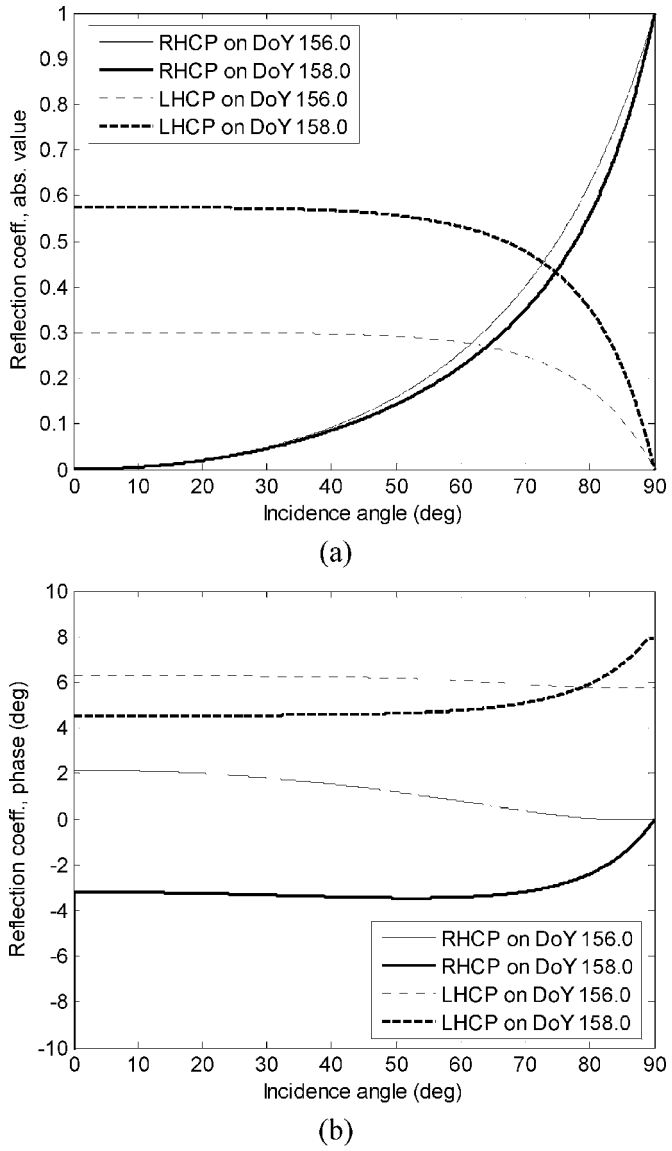

Fig. 5. Reflection coefficients at two circular polarizations for the cases of the profile shown in Fig. 4(a) and (b); (a) corresponds to amplitude and (b) to phase of the reflection coefficient.

$S_n(\pm\theta)$ was not available for the type of antennas used in the experiment. As a proxy we used phase data available for us for a similar type of geodetic antenna. Practically, what matters for this problem is the difference between phases at two opposite circular polarizations, which is about 90°. We should note that such behavior of antenna patterns at opposite polarizations was required for the moisture-induced modulation phase shift to be clearly observed. Increase in soil moisture would lead to an increase in reflectivity for LHCP and a corresponding decrease for RHCP. Because of the specific values of the power gains at low elevation angles, such an increase changes the balance between values A_1 and A_2 from (17)–(18), leading to a noticeable change in phase $\Psi(\theta)$. We found from our simulations that by altering antenna pattern characteristics (both the amplitude and the phase), the effect of the modulation phase shift due to soil moisture can be reduced below levels observed in the experiment.

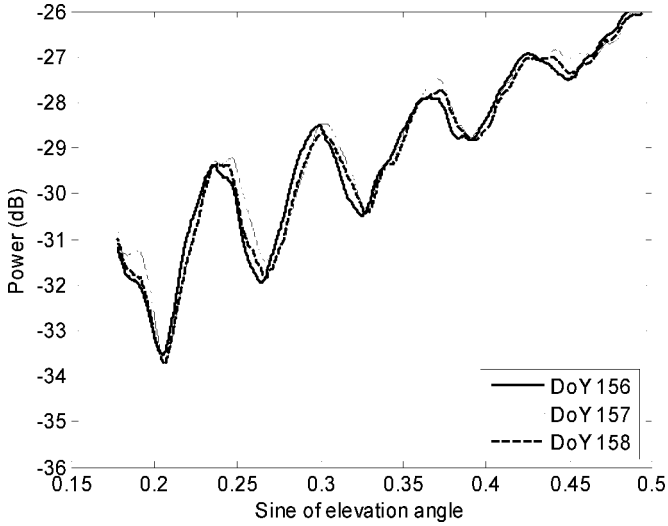

Fig. 6. Observed modulation patterns for three consecutive times (DoY 156, 157, and 158), before, during, and after the precipitation event.

Analysis of (12) and (13) shows that the modulation amplitude, $|A(\theta)|$, and the phase shift, $\Psi(\theta)$, depend on the combined interaction between antenna gains and reflection coefficients including both their amplitudes and phases. Fig. 5(a) contains information which is very important for understanding the modulation phase shift used to model VWC in [1], [2]. Since the observed modulation is confined to elevation angles between $\sim$ 5 to 30°, special attention should be paid to the behavior of the reflection-coefficient amplitude in Fig. 5(a) in the interval of incidence angles from 60° to 85°. Over this interval, rain creates a substantial change in LHCP reflection coefficient but only minor changes in RHCP reflection coefficient. Thus, the modulation phase shift critically depends on the relationship between the amplitudes of reflection coefficients at different polarizations combined with the antenna pattern behavior at the same angles.

B. Comparisons Between Observed and Modeled Modulation Patterns

Now we can move to the central point of this work, a comparison between the observed and modeled modulation patterns. In Fig. 6, the observed modulation patterns are shown for three consecutive times (DoY 156, 157, and 158), before, during, and after the rain event. First, a noticeable shift in modulation phase to the right is seen. For convenience, a vertical scale is chosen to closely match the data with modeled curves, since we are not concerned with absolute values.

Fig. 7(a) shows a comparison between two theoretical SNR curves for DoY 156 and a rain event on DoY 158. Very similar curves were obtained for another rain event, around DoY 229, shown in Fig. 7(b). One can see that both the experimental and theoretical curves have the same number of maxima (or minima) over the same range of elevation angles, and the magnitudes of SNR oscillations are of the same order. More importantly, the phase shift caused by the increase in soil moisture has the correct sign and is of the same order of magnitude. The average slope of the corresponding curves differs somewhat, which can be attributed to the uncertainty of the soil model, or in the knowledge

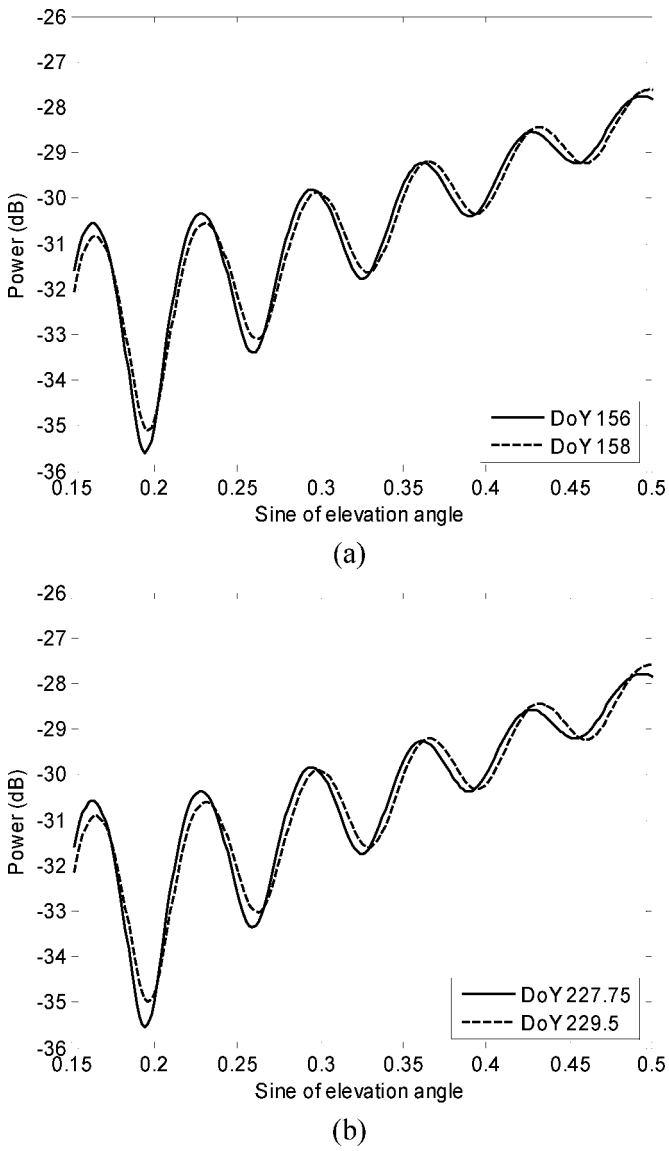

Fig. 7. Calculated SNR modulation curves based on soil moisture profiles measured on (a) DoY 156 and DoY 158, and on (b) DoY 227.75 and DoY 229.5.

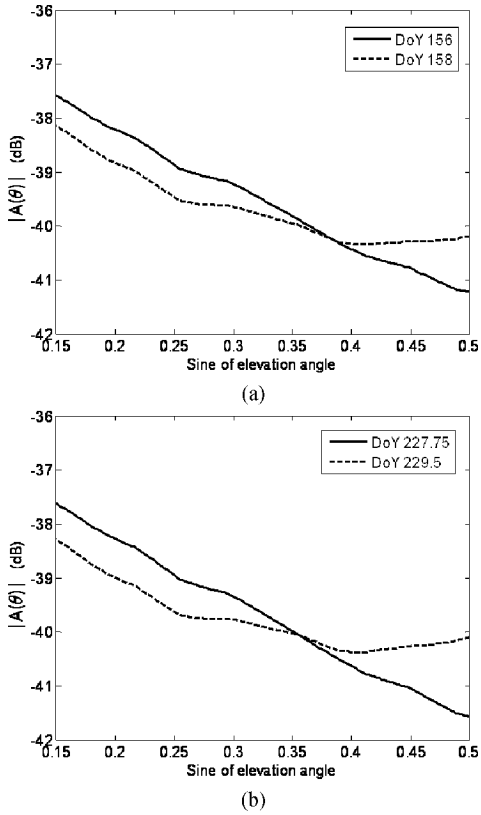

Fig. 8. Amplitude $|A(\theta)|$ calculated for soil moisture profiles measured on (a) DoY 156 and DoY 158, and on (b) DoY 227.75 and DoY 229.5.

of the antenna patterns. This issue should be addressed in future studies.

Sensitivity of the modulation pattern to the change in soil moisture can be illustrated by plotting parameters $|A(\theta)|$ and $\Psi(\theta)$ as a function of sine of elevation angle θ for dry and wet days. These curves are presented in Figs. 8 and 9. It is seen that $|A(\theta)|$ changes noticeably with angle, which was also observed in the experiment [Fig. 1(b)]. Phase $\Psi(\theta)$ also changes with the angle but as we will see later, this change is close to $\sin\theta$. More importantly, while both characteristics are sensitive to change in soil moisture, they show this sensitivity quite differently. Whereas a transition from dry to wet conditions gives a negative offset to $\Psi(\theta)$ of the order of 20° monotonically for the entire range of elevation angles between 5° to 30°, change of $|A(\theta)|$ has a different sign for angles below and above $\sim 20°$. Most likely this peculiarity reflects the interplay between antenna gains and reflection coefficients at different polarizations for this range of negative elevation angles. This behavior of $|A(\theta)|$ should be taken into account if the estimates of soil moisture are based on modulation amplitude rather than modulation phase.

Intuitively, the modulation phase shift Ψ can be thought of as being produced by the effect of signal penetration into soil. Indeed, since in (3)Ψ appears as an addition to the geometric phase $\Phi = k\Delta l = 2kh\sin\theta$, one may regard the value $\Delta h = \Psi/2k\sin\theta$ as a penetration depth. However, the phase Ψ is a rather complicated combination of different parameters related both to antenna gain and soil reflectivity, so in [1] and [2], we call it an effective reflector depth rather than a penetration depth. Therefore, only a change in Δh with a corresponding change of soil moisture can be attributed to some sort of penetration. Interestingly, while Ψ changes monotonically over θ, Δh remains practically constant. This behavior is seen in Fig. 10(a) and (b). First, one can see that $|\Delta h|$ decreases only slightly from 6 cm to 5 cm with decreasing elevation angle. This explains the success of the retrieval algorithm presented in [1] and [2], where modulation data were approximated by the function $\cos[2k(h+\Delta h)\sin\theta]$, where Δh was chosen as a constant for a specific measurement. Actually, the absolute value of Δh cannot be retrieved from these measurements, only a difference $\delta h = \Delta h_{dry} - \Delta h_{wet}$ between two measurements of Δh, with a maximal value of ~ 5 cm observed at Marshall [1], [2]. We also can estimate $\delta h_{\max}$ from our numerical modeling. From Fig. 10, it follows that for that particular event around DoY 157, one would expect a relative change of $\delta h_{\max} \approx 2$ cm.

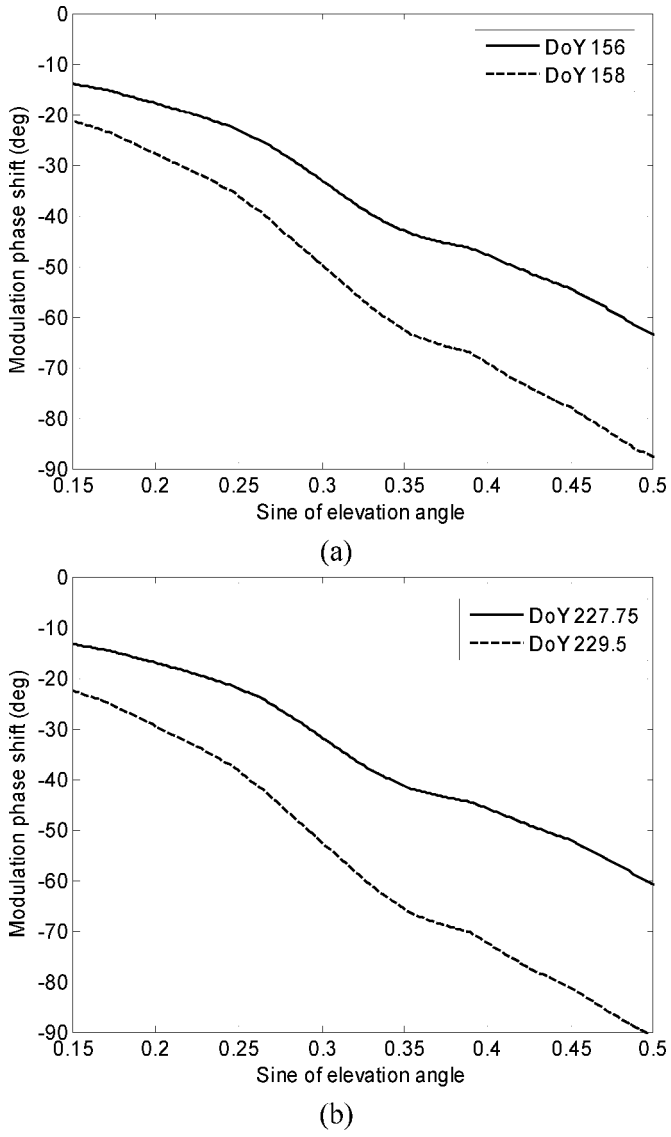

Fig. 9. Phase $\Psi(\theta)$ calculated for soil moisture profiles measured on (a) DoY 156 and DoY 158, and on (b) DoY 227.75 and DoY 229.5.

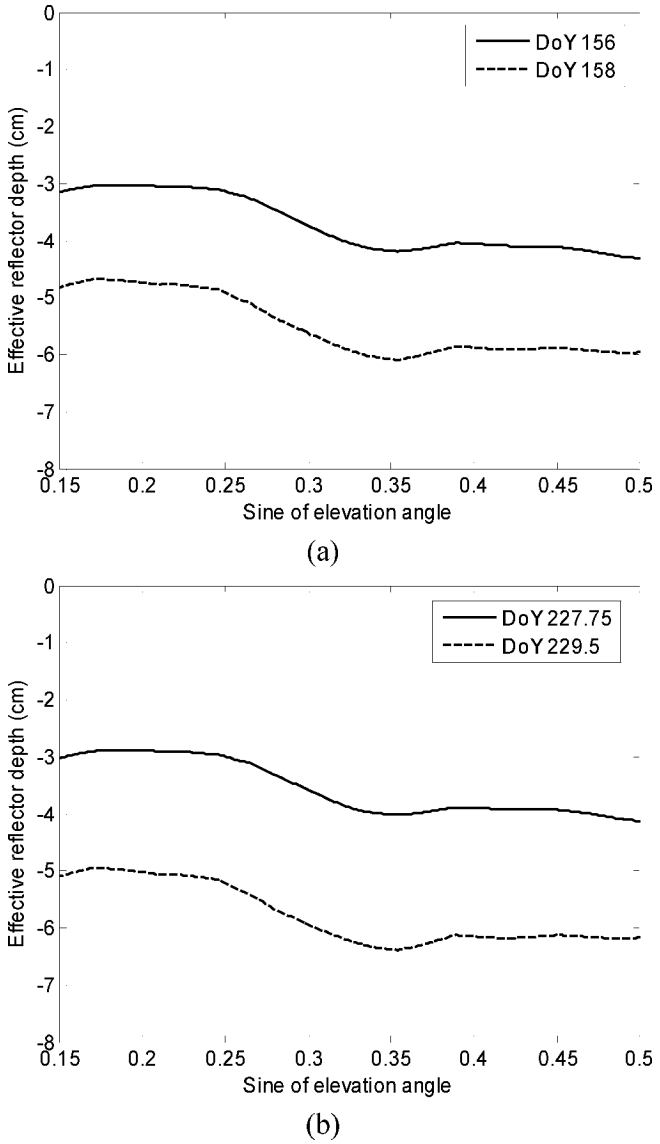

Fig. 10. Effective reflector depth $\Delta h(\theta)$ calculated for soil moisture profiles measured on (a) DoY 156 and DoY 158, and on (b) DoY 227.75 and DoY 229.5.

Although Ψ is only indirectly related to the penetration depth, there are other ways to obtain the GPS signal penetration depth. It is possible to calculate transmission coefficients as a function of depth instead of reflection coefficients and estimate the penetration depth from them, but this is a more cumbersome task. Because we have an algorithm based on reflection coefficients on hand, we simplify the scenario as a strong planar reflector located at various depths and analyze the sensitivity of the modulation pattern.

For this, we simulated the SNR modulation pattern for the case of a metal (highly conductive) layer buried in the soil at some depth. For the soil profiles, we used profiles previously employed for this study, simply assigning high values of ε ($\sim 10^6$) to the medium lying below some depth. The SNR modulation calculations were performed for various depths. We defined a physical penetration depth of the GPS signal as a depth of the buried reflecting plate at which one can start seeing the difference between SNR with and without the plate. It was found that for silty clay and dry conditions, the penetration depth Δh is about 10 cm, and for wet conditions Δh is about 5 cm, giving $\delta h \sim 5$ cm, approximately the maximal δh observed in the experiment [2].

V. Conclusion

This paper presented a model of GPS surface multipath for the case of bare soil with a plane surface. The soil was modeled as a layered dielectric medium with losses. Reflection coefficients from the upper interface of such media were calculated using a robust numerical algorithm based on the known theory. Representative antenna gain patterns have been used in the calculations of direct and reflected polarized signals. We demonstrated that reasonable soil moisture profiles for dry and wet conditions output modulation patterns similar to those obtained in the experiment [1], [2] with both the correct sign for the phase shift and of the same order of magnitude.

As was shown in Section I, the shift of the modulation phase is a quite complicated function of various factors such as antenna gains, their phases, and also of the magnitudes of reflection coefficients related to various degrees of the soil wetness. The behavior of reflection coefficients shows that they are quite sensitive to the behavior of dielectric permittivity in the top 5 cm. The concept of an "effective reflector depth" used in [1] and [2] is supported by the theoretical modeling. Nevertheless, the connection between soil moisture and the physical penetration depth of the L-band radiation into the soil is quite complicated. Another parameter of the modulation pattern, its amplitude, also depends on changes in soil moisture, though it is a less convenient measurement for moisture retrievals because of its nonmonotonic behavior with elevation angle.

It should be noted that any real land surface has variations of heights, at least of the order of a few centimeters. The same can be said about variations of soil moisture over depth. An approximation of a real medium with a layered medium means that such a model should account for averaging out variations of soil moisture over some depth associated with the standard deviation of the equi-moist surface. Such an average would be very critical for the volume where both top soil and air are involved. Even without implementing these additional levels of complication, the analysis presented gives a plausible explanation for the observational data obtained in [1] and [2]. It also demonstrates the feasibility of using ground-based GPS receivers for soil moisture estimates, provided they are properly calibrated. We have also shown that viable calibrations will be specific to the antenna pattern, due to the dependence of modulation amplitude and phase on the receiving antenna's RHCP and LHCP patterns.

Here we used semiempirical relationships developed in [8] that relate real and imaginary parts of ε for L-band to the volumetric water content (VWC) in soil. One of the limitations of such a model is that it used the concept of out-of-soil water in order to predict frequency dispersion of the soil dielectric properties. More advanced dielectric models for moist soils have been proposed since then which account for bound soil water (see, e.g., [20] and [21]). It would be very instructive to test those new models for the case of GPS signal reflections from soil.

In this paper, we considered a rather idealized situation of bare soil/flat surface environment. We did not include the effects of vegetation and surface topography due to the complexity of the current problem of modeling the signal output by a geodetic antenna receiving both direct and reflected GPS signals at both orthogonal circular polarizations in the presence of a stratified soil. Calculations show that the geometric optics approach used to model reflected signals is quite robust and does not pose strict limitations. Above we outlined how the effect of small-scale surface roughness (which reduces the coherence of the reflected wave) can be rather straightforwardly handled within this geometric optics approach, and that could be the next step to improve the model.

After studying this phenomenon at the current idealized level, we can proceed toward a more elaborate model. In order to obtain a better quantitative agreement between experiment and theory, more accurate *in situ* soil moisture measurements under controllable surface topography conditions and thorough modeling of vegetation are required. Our experimental results were limited to data from a single site (Marshall, CO) and will need to be tested elsewhere. In terms of topography, the surface is on average nearly horizontal. Animal burrowing is the primary source of surface roughness on the otherwise plane surface, yielding broad mounds less than 10 cm in height separated by a distance of several meters. More accurate quantitative description of the surface at this time was not available. Vegetation at the site is sparse and is classified as short-grass steppe. The biomass (canopy plus litter) of this vegetation was not available. Since the site was not exactly bare, it is not clear what effect this may have had on bare soil model results. From what is already known in the literature [23], [24], vegetation leads to the signal absorption and further reduction of the L-band signal coherence due to a diffusive volume scattering in the layer of vegetation in the presence of the soil surface. Approaches that handle scattering by vegetation have been developed in passive microwave radiometry and radar scatterometry [22], [23], and may be useful for the modeling of the GPS signal scattering.

ACKNOWLEDGMENT

The authors would like to thank UNAVCO and J. Normandeau for field and archiving support, the NCAR RAL Group at Marshall for providing precipitation data, and the anonymous reviewers and editors whose comments improved this manuscript.

REFERENCES

[1] K. M. Larson, E. E. Small, E. Gutmann, A. Bilich, J. Braun, and V. Zavorotny, "Use of GPS receivers as a soil moisture network for water cycle studies," *Geophys. Res. Lett.*, vol. 35, no. DOI:10.1029/2008GL036013, p. L24405, 2008.

[2] K. M. Larson, J. J. Braun, E. E. Small, V. U. Zavorotny, E. Gutmann, and A. L. Bilich, "GPS multipath and its relation to near-surface soil moisture content," *IEEE J. Sel. Topics Appl. Earth Obs. Remote Sens.*, vol. 3, no. 1, Mar. 2010.

[3] E. G. Njoku and D. Entekhabi, "Passive microwave remote sensing of soil moisture," *J. Hydrol.*, vol. 184, no. 1, pp. 101–130, 1996.

[4] J.-P. Wigneron, J.-C. Calvet, T. Pellarin, A. A. Van de Griend, M. Berger, and P. Ferrazzoli, "Retrieving near-surface soil moisture from microwave radiometric observations: Current status and future plans," *Remote Sens. Environ.*, vol. 85, pp. 489–506, 2003.

[5] B. W. Parkinson, J. J. Spilker, P. Axelrad, and P. Enge, Eds., Global Positioning System: Theory and Applications, Washington, DC, 1996, vol. I, American Institute of Aeronautics and Astronautics.

[6] V. U. Zavorotny and A. G. Voronovich, "Scattering of GPS signals from the ocean with wind remote sensing application," *IEEE Trans Geosci. Remote Sensing*, vol. 38, no. 3, pp. 951–964, Mar. 2000.

[7] M. T. Hallikainen, F. T. Ulaby, M. C. Dobson, M. A. El-Rayes, and L.-K. Wu, "Microwave dielectric behavior of wet soil—Part I: Empirical model and experimental observations," *IEEE Trans. Geosci. Remote Sens.*, vol. GRS-23, no. 1, pp. 25–34, Jan. 1985.

[8] M. T. Hallikainen, F. T. Ulaby, M. C. Dobson, M. A. El-Rayes, and L.-K. Wu, "Microwave dielectric behavior of wet soil—Part II: Dielectric mixing models," *IEEE Trans. Geosci. Remote Sens.*, vol. 23, no. 1, pp. 35–44, Jan. 1985.

[9] N. R. Peplinski, F. T. Ulaby, and M. C. Dobson, "Dielectric properties of soils in the 0.3–1.3-GHz range," *IEEE Trans. Geosci. Remote Sens.*, vol. 33, no. 5, pp. 803–807, May 1995.

[10] L. M. Brekhovskikh, *Waves in Layered Media*. New York: Academic, 1960.

[11] J. R. Wait, *Electromagnetic Waves in Stratified Media*. New York: Pergamon, 1962.

[12] F. T. Ulaby, R. K. Moore, and A. K. Fung, *Microwave Remote Sensing: Active and Passive*. Reading, MA: Addison-Wesley, 1981, vol. 1.

[13] L. Tsang, J. A. Kong, and R. T. Shin, *Theory of Microwave Remote Sensing*. New York: Wiley-Interscience, 1985.

[14] A. Ishimaru, *Electromagnetic Wave Propagation, Radiation, and Scattering*. Englewood Cliffs, NJ: Prentice-Hall, 1991.
[15] I. M. Fuks and A. G. Voronovich, "Wave diffraction by rough interfaces in an arbitrary plane-layered medium," *Waves Random Media*, vol. 10, pp. 253–272, 2000.
[16] J. M. Wraith and D. Or, "Temperature effects on soil bulk dielectric permittivity measured by time domain reflectometry: Experimental evidence and hypothesis development," *Water Resour. Res.*, vol. 35, no. 2, pp. 361–369, 1999.
[17] P. A. Ferre, J. H. Knight, D. L. Rudolph, and R. G. Kachanoski, "The sample areas of conventional and alternative time domain reflectometry probes," *Water Resour. Res.*, vol. 34, no. 11, pp. 2971–2979, 1998.
[18] S. Kurc and E. Small, "Soil moisture variations and ecosystem-scale fluxes of water and carbon in semiarid grassland and shrubland," *Water Resour. Res.*, vol. 43, no. DOI:10.1029/2006WR005011, p. W06416, 2007.
[19] F. Chen and J. Dudhia, "Coupling an advanced land surface-hydrology model with the Penn State-NCAR MM5 modeling system. Part I: Model implementation and sensitivity," *Mon. Weather Rev.*, vol. 129, pp. 569–585, 2001.
[20] D. Or and J. M. Wraith, "Temperature effects on soil bulk dielectric permittivity measured by time domain reflectometry: A physical model," *Water Resour. Res.*, vol. 35, no. 2, pp. 371–383, 1999.
[21] V. L. Mironov, M. C. Dobson, V. H. Kaupp, S. A. Komarov, and V. N. Kleshchenko, "Generalized refractive mixing dielectric model for moist soils," *IEEE Trans. Geosci. Remote Sens.*, vol. 42, pp. 773–785, 2004.
[22] Y. Du, F. T. Ulaby, and M. C. Dobson, "Sensitivity to soil moisture by active and passive microwave sensors," *IEEE Trans. Geosci. Remote Sens.*, vol. 38, no. 1, pp. 105–113, Jan. 2000.
[23] R. D. De Roo, Y. Du, F. T. Ulaby, and M. C. Dobson, "A semi-empirical backscattering model at L-band and C-band for a soybean canopy with soil moisture inversion," *IEEE Trans. Geosci. Remote Sensing*, vol. 39, no. 4, pp. 864–872, Apr. 2001.

Valery U. Zavorotny (M'01–SM'03) received the M.Sc. degree in radio physics from Gorky State University, Gorky, Russia, in 1971, and the Ph.D. degree in physics and mathematics from the Institute of Atmospheric Physics, USSR Academy of Sciences, Moscow, in 1979.

From 1971 to 1990, he was a Research Scientist with the Institute of Atmospheric Physics of the USSR Academy of Sciences, Moscow. In 1990, he joined Lebedev Physical Institute, Moscow, Russia. In 1991–2000, he was a CIRES Research Associate in the Environmental Technology Laboratory of the National Oceanic and Atmospheric Administration (NOAA), Boulder, CO, and became a NOAA/ETL physicist in 2000. His research interests include theory of wave propagation through random media, wave scattering from rough surfaces, and ocean and land remote sensing applications.

Dr. Zavorotny is a member of URSI (Commission F) and the American Geophysical Union.

Kristine M. Larson received the B.A. degree in engineering sciences from Harvard University, Cambridge, MA, in 1985, and the Ph.D. degree in geophysics from the Scripps Institution of Oceanography, University of California at San Diego, La Jolla, in 1990.

She was a member of the technical staff at JPL from 1988–1990. Since 1990, she has been a professor in the Department of Aerospace Engineering Sciences, University of Colorado, Boulder. Her research interests are focused on developing new applications and techniques for GPS.

John J. Braun received the B.A. degree in physics and mathematics in 1991 from the University of Colorado, Boulder, and the PhD. degree from the Department of Aerospace Engineering Sciences, University of Colorado, in 2004.

He is a project scientist within the COSMIC program at the University Corporation for Atmospheric Research, Boulder. His research interests include developing new techniques and using GNSS observations to study the Earth and its environment, particularly the water cycle.

Eric E. Small received a B.A. degree in geological sciences from Williams College in 1993 and the Ph.D. degree in earth sciences from the University of California at Santa Cruz in 1993.

He is an Associate Professor in the Department of Geological Sciences, University of Colorado, Boulder. His research is focused on land surface hydrology.

Ethan D. Gutmann received the B.A. degree in geology and computer science from Williams College in 1999 and the Ph.D. degree in geological sciences from the University of Colorado, Boulder, in 2008.

He is a postdoctoral fellow at the Research Applications Laboratory, National Center for Atmospheric Research, Boulder.

Andria L. Bilich received the B.S. degree in geophysics from the University of Texas, Austin, in 1999, and the Ph.D. degree in aerospace engineering sciences from the University of Colorado, Boulder, in 2006.

She is a Geodesist with the National Geodetic Survey's Geosciences Research Division. Her research interests include GPS multipath characterization, GNSS antenna calibration, and precision improvements to GNSS positioning for geoscience applications.